Micron 73 (2015) 9–14

Contents lists available at ScienceDirect

Micron

journal homepage: www.elsevier.com/locate/micron

Electronic structure of MgS and $MgYb_2S_4$: Electron Energy-Loss Spectroscopy and self-consistent multiple scattering calculations

M.S. Moreno [a,*], Esteban Urones-Garrote [b], L.C. Otero-Díaz [c]

[a] Centro Atómico Bariloche, 8400, San Carlos de Bariloche, Argentina
[b] Centro Nacional de Microscopía Electrónica, Universidad Complutense, Madrid, E-28040, Spain
[c] Departamento de Química Inorgánica, Facultad de Ciencias Químicas, Universidad Complutense, Madrid, E-28040, Spain

ARTICLE INFO

Article history:
Received 15 January 2015
Received in revised form 13 March 2015
Accepted 13 March 2015
Available online 23 March 2015

Keywords:
Sulfides
EELS
Electronic structure
Multiple scattering calculations

ABSTRACT

The electronic structure of MgS and $MgYb_2S_4$ have been studied using the fine structure of the Mg-K, S-K, Mg-$L_{2,3}$, S-$L_{2,3}$ and Yb-N_5 edges measured by electron energy-loss spectroscopy (EELS). Our experimental results are compared with real-space full multiple scattering calculations as incorporated in the FEFF9.6 code. All edges are very well reproduced. Total and partial densities of states have been calculated. The calculated densities of states of Mg and S are similar in both compounds. The energy distribution of these states suggests a covalent nature for both materials. For $MgYb_2S_4$ a band gap smaller than for MgS is predicted. In this compound the top of the valence band and the bottom of the conduction band are dominated by Yb states.

1. Introduction

Sulfides are of interest for a broad range of applications (Gao et al., 2013). Transition metal dichalcogenides have been proposed as potential alternatives to graphene (Johari and Shenoy, 2012). Sulfide composites are under intense search as promising cathodes in Li–S batteries (Su and Manthiram, 2012; Cai et al., 2012). Sulfide-based luminescent materials are known to have electronic properties that make them of interest for a range of applications, for example as inorganic pigments among others. Several monochalcogenides are included in this class of materials (Smet et al., 2010), like CdS and CaS. Solid solutions of these compounds with the NaCl-type crystal structure also shows photoluminescent properties (Barrett et al., 2005). MgS presents this crystal structure type and can form solid solutions with CdS (Poole et al., 1997).

Other structural possibilities can be found in combination with other stoichiometries. One well documented example is the formation of MS–R_2S_3 solid solutions (M: alkaline-earth metal; R: rare-earth metal) (Flahaut, 1979), adopting NaCl-type and related superstructures for M = Ca or Mg and for the heavy rare-earth metals. The MgS–Yb_2S_3 system can be formulated as $Mg_{1-x}Yb_{(2/3)x}\square_{(1/3)x}S$ ($0 \le x \le 0.75$), where □ = cation vacancies. The solid solution for M = Mg and R = Yb was characterized in detail recently due to its potential properties as environmentally-friendly inorganic pigments (Urones-Garrote et al., 2004; Urones-Garrote et al., 2005). The system presents exclusively the NaCl-type structure for $x \le 0.30$ and above that nominal composition the existence of crystals with spinel-type structure is also detected employing TEM and associated techniques. The coexistence of both structure types can be attributed to an order–disorder transition from NaCl-type into spinel-type, since they share the same basic framework, which is the structure of atacamite ($Cu_2(OH)_3Cl$, with a B_2X_4 stoichiometry) (Urones-Garrote et al., 2005). Electron diffraction studies show the existence of intense diffuse scattered intensity in the NaCl-type crystals that can be attributed to short-range effects in the cation sublattice (Withers et al., 2007). Interestingly the local coordination for Mg and S changes from octahedral in the NaCl-type structure to tetrahedral in the spinel structure. In consequence variations in the properties are expected due to this change in the crystal structure. In fact, MgS is white whilst $MgYb_2S_4$ has a green colour, suggesting modifications in the electronic properties.

In order to distinguish each phase individually and to follow the evolution of the solid solutions we need robust methods for the characterization of the end members of the solution. Electron microscopy provides a spatial resolution adequate to distinguish each phase, even in multiphasic samples. In addition to its bulk sensitivity, electron energy-loss spectroscopy (EELS) implicitly contains local structural, chemical and electronic information. The different absorption edges in the spectrum correspond to excitations from core electron levels of particular atoms in the sample. In

* Corresponding author.
E-mail address: smoreno@cab.cnea.gov.ar (M.S. Moreno).

http://dx.doi.org/10.1016/j.micron.2015.03.005
0968-4328/

particular, an added advantage is that (in many cases) the observed EEL spectrum exhibits a structure that is highly sensitive to the nature of the chemical bonds and specific to the local nearest-neighbor coordination around the excited atom, and can be used as a coordination fingerprint (Egerton, 2011). This fine structure is also related to the electronic structure in terms of the site- and symmetry-projected density of unoccupied states (local projected density of states, LDOS).

It can be expected that the energy-loss near-edge structure (ELNES) of S-K and Mg-K edges be sensitive to coordination variations and allow to distinguish between MgS and $MgYb_2S_4$ phases. We are aware of the study of S-K edge in MgS by XAS (Kravtsova et al., 2004; Fleet, 2005) but reports about the Mg-K edge are limited to those in Urones-Garrote et al. (2005). The compound $MgYb_2S_4$ seems not to have being studied yet by XAS and EELS studies are limited to the Mg-K edge (Urones-Garrote et al., 2005). The Mg-K edge for the composition $x = 0.30$ of the solid solution can be found in Fig. 4 of Urones-Garrote et al. (2005). The main difference with the end members appears at about 10 eV above threshold, with an intermediate fine structure and intensity due to the order–disorder transition from NaCl to spinel-type structure. A similar situation is found about theoretical calculations, the MgS phase have been studied by using a multiple scattering (Kravtsova et al., 2004) approach as implemented in G4XANES and ground state calculations (Chen et al., 2009; Khan et al., 2012; Drief et al., 2004) have reported DOS, but we are not aware of any calculation of the electronic structure for the compound $MgYb_2S_4$.

The purpose of this work is the experimental and theoretical study of the electronic structure of MgS and spinel-type $MgYb_2S_4$ compounds (end members of the solid solution mentioned above) through the ELNES fine structure present in the edges available in EEL spectroscopy that can provide relevant information about the electronic structure, that is Mg-K, S-K, Mg-$L_{2,3}$, S-$L_{2,3}$ and Yb N_5 edges together with the study of the energy distribution of electronic states of different symmetry of the constituent atoms of these sulfide compounds, and the calculation of the EELS spectrum using the FEFF code.

2. Materials and methods

The samples (MgS and $MgYb_2S_4$) were synthesized – using as precursors the corresponding nitrates $Mg(NO_3)_2{\cdot}6H_2O$ and $Yb(NO_3)_3{\cdot}5H_2O$ – under a flow of H_2S (10% in Ar) and a flow of Ar bubbling in CS_2 at a temperature of 1000 °C for 10 h. The compositions were checked by EDS analysis. By electron diffraction we checked that no other feature than Bragg reflections were present. See Urones-Garrote et al. (2005) for details.

TEM observations were performed in a Philips CM200FEG electron microscope fitted with a GIF 200. EEL spectra were acquired in diffraction mode, with a collection semi-angle of ~4.6 mrad, a dispersion of 0.1 eV/pixel and an acquisition time of 8 s. The energy resolution was ~0.9 eV, measured from the FWHM of the zero-loss peak. More than 15 spectra from S-K and Mg-K edges were collected from each metal sulfide and added after alignment.

Sample stability under the electron beam was checked by looking to the diffraction pattern after irradiation with a similar dose to the supplied for core loss acquisition. We have not found changes in the diffraction pattern of both materials under the conditions tested.

3. Calculations

To correlate ELNES spectral features with metal and S contributions, the Mg-K and S-K edges were calculated by means of FEFF program. Calculations using this approach are based on the multiple scattering theory. Accurate and well converged potentials and electron densities are calculated in a self-consistent-field (SCF) procedure (Ankudinov et al., 1998). Version FEFF9.6 allows to take into account experimental parameters in EELS such as beam energy, convergence and collection semiangles and sample to beam orientation (Rehr et al., 2010). Convergence of the calculations can be evaluated by changing the size of the cluster used (Moreno et al., 2007). For some systems real-space calculations can be time consuming because of the need of a large cluster of atoms. A combined real and k-space approach can be used to ensure convergence (Jorissen and Rehr, 2010). In this work we used both approaches to obtain well converged calculations. The FEFF calculations were done with the Hedin–Lungqvist self-energy (i.e., complex exchange correlation potentials) to account for inelastic losses. In the construction of the muffin-tin potentials, we allowed for different degrees of overlapping of the muffin-tins in order to reduce discontinuity effects at the edges of the muffin-tins and to roughly determine the need for nonspherical corrections to the potentials. We found that a cluster of about 60 atoms was sufficient to obtain well converged potentials. The UNFREEZEF card was used to include the Yb f states in the SCF calculation providing their accurate energy position. For the full multiple scattering (FMS) calculations, a cluster size was used and tested for convergence. Typically a cluster of more than 200 atoms was enough. We have also considered the presence of final-state effects in the observed edges, resulting from the core-level excitation. This core–hole effect is approximated using the RPA approximation.

4. Results and discussion

In Fig. 1 are shown the calculated density of states (DOS) for MgS and its *l*-projected components projected on the magnesium

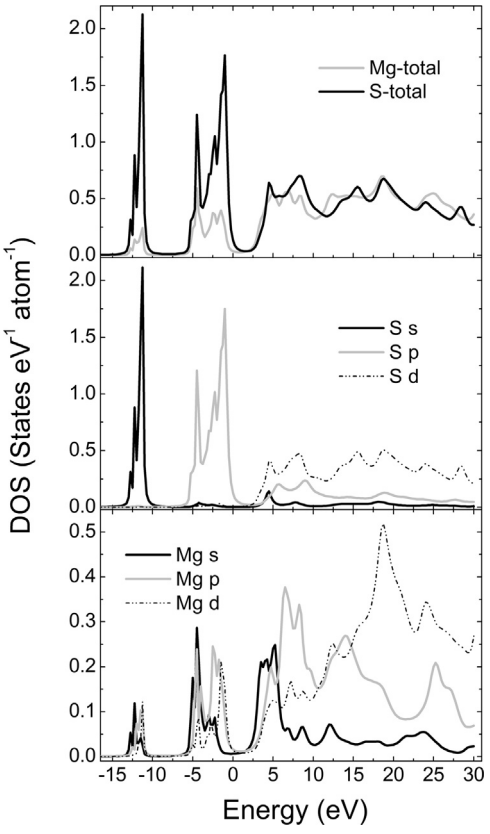

Fig. 1. Calculated partial densities of states at the sulfur and magnesium site in MgS. The zero of energy is the Fermi level.

and sulfur sites, respectively, within a 46 eV range. Note the similar scales of the vertical axes for the total sulfur and magnesium DOS above Fermi level and the significant contribution from sulfur and magnesium at both sides of the Fermi level, indicating a covalent nature of MgS. Structures occur in the S and in the Mg partial DOS at the same energies, a good indication that hybridization must play an important role in MgS.

It is seen that the valence band is mainly formed by S p states, while the band centered at about −12.5 eV is formed of s-states of S. Both structures are contributed by Mg s, p and d states. Mg p and d states contribute to the upper portion of the valence band. Our densities of states are in agreement with previous calculations obtained using multiple scattering (Kravtsova et al., 2004) and ground state calculations (Chen et al., 2009; Khan et al., 2012; Drief et al., 2004).

In the conduction band the sulfur DOS has a 3p and 3d character up to 10 eV above the Fermi level, being the d states the dominant contribution above this energy. The s states contribute mainly to the first 5 eV above Fermi level. This quite large spread in energy of the spectral features with sulfur 3p character is an indication of strong covalency in this material. The first peak in the Mg DOS is almost equally contributed by 3s, 3p and 3d states up to 5 eV, while those at 6–7 eV are mostly of p and d character. These features indicate the existence of hybridization between the 3s, 3p and 3d states. The total Mg DOS is mainly of p and d character above 5 eV, becoming the d contribution the dominant one above 15 eV. In consequence we divide the spectra into two regions: the first, involving the first 5 eV, is attributed to hibridization of sulfur 3p and 3d states with metal states of 3s, 3p and 3d character. A second region, above 5 eV after threshold, is attributed to sulfur p-d character hybridized with magnesium 3p and 3d states.

Note that the band gap is bounded by S p states in the valence band, with a minor contribution of Mg p and d states, and Mg s states and S d states in the conduction band. The estimated band gap is about 2.6 eV in agreement with calculations using LAPW, FP-LAPW, TBLMTO and pseudopotential (GGA) which predict an indirect band gap of approximately the same value (Chen et al., 2009; Khan et al., 2012; Drief et al., 2004; Stepanyuk et al., 1992; Kalpana et al., 1996).

In Fig. 2 are shown the corresponding DOS for $MgYb_2S_4$ within a 45 eV range. The presence of a band gap can be realized. Its magnitude is about 1 eV narrower than for MgS. This trend is in agreement with the observed colour for this compound.

Following the previous considerations, a close similarity to MgS for Mg and S contributions can be realized. The description is rather equivalent to that for MgS, the main difference being that the Mg *s* states contributes more significantly to the DOS in the conduction band up to 10 eV.

The calculated density of states reveals a covalent nature of these phases. The structures appearing within the first 10 eV above threshold arise from a covalent mixing of mainly S 2p and Mg s–p (plus Yb in $MgYb_2S_4$) states. It is obvious that the band centered at about −12 eV on the curves of the total DOS of MgS and $MgYb_2S_4$ originates mainly from contributions of S 2s states with minor but not negligible contributions of s, p and d states of Mg and Yb atoms.

The main difference between the electronic structure of MgS and $MgYb_2S_4$ is the presence in the valence band of $MgYb_2S_4$ of a strong band associated with contributions of the Yb 4f states. The Yb f states are included in the Yb total DOS shown in the upper panel of Fig. 2. The contribution to this band dominates the intensity at the top of the valence band of $MgYb_2S_4$, with a minor contribution of S states. The Yb d states are also the main contributors to the conduction band up to about 12 eV. The band gap in consequence is bounded by Yb states. An important prediction of our results is that the band gap is narrower in this compound compared to MgS, being the Yb states responsible for such reduction. The estimated value for the band gap is about 1.6 eV, almost 1 eV less than for

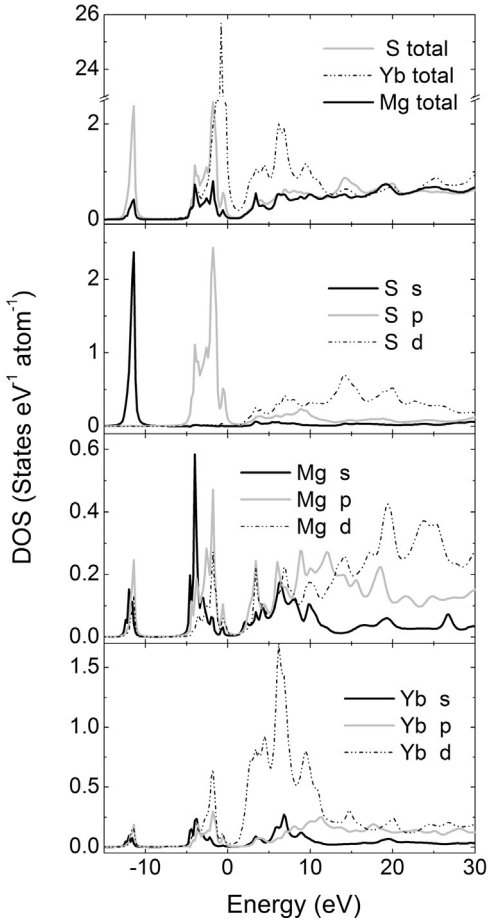

Fig. 2. Calculated partial densities of states at the sulfur, yterbium and magnesium site in $MgYb_2S_4$. The zero of energy is the Fermi level.

MgS. In the lack of an experimental measurement or other theoretical calculations of the electronic structure of this material this value is the first estimation for the band gap. The values of band gaps calculated within the FEFF program are known to be underestimated (Ankudinov et al., 1998). In ternary Hf oxides it has been demostrated that the position of the Hf f sub-band is underestimated by several eV with respect to the Fermi energy (Lavrentyev et al., 2011). However the green colour of $MgYb_2S_4$ is an indication of a band gap smaller than that for MgS suggesting that a possible shift in the Yb sub-band if happen should still leave it close to the Fermi level.

These results suggest that the band gap values could change with compositional variations in the solid solution, in agreement with the different colours of the end members. Changes in the band gap of MgS with doping have been calculated recently but more importantly it was found that its nature is modified by doping with Te or Se passing from indirect to direct band gaps, making MgS optically active (Khan et al., 2012).

The EEL spectra acquired over a broad energy range for MgS and $MgYb_2S_4$ are shown in Figs. 3–6 respectively. For MgS the S K-edge agree with the XAS data reported by Kravtsova et al. (2004) and Fleet (2005). This agreement provides additional evidence that radiation damage was not present in this compound under the experimental conditions used.

These spectra are compared with the corresponding calculated S-K, Mg-K, Mg-$L_{2,3}$, S-$L_{2,3}$ and Yb-N_5 spectra. For comparison are included spectra obtained by taking into account core–hole effects and without it. In all these calculations the experimental conditions have been considered. It can be realized that in all cases a very

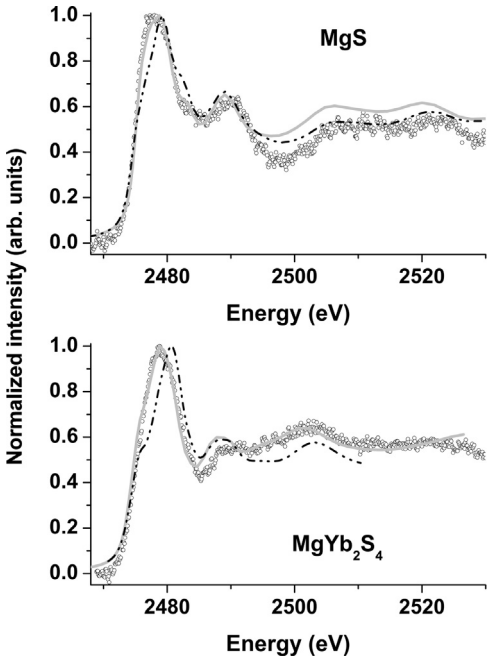

Fig. 3. Sulfur *K*-edge in MgS and $MgYb_2S_4$. Experimental: open circles. Calculated: solid gray line includes core–hole effects, dash-dot line does not include core–hole effects.

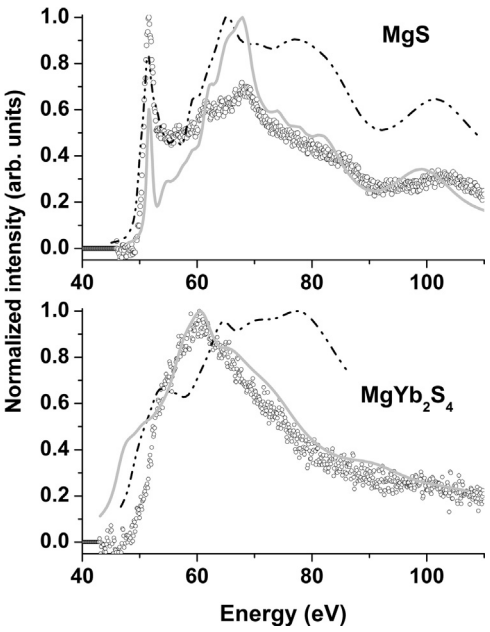

Fig. 5. Mg L_{23}-edges in MgS and $MgYb_2S_4$. Experimental: open circles. Calculated: solid gray line includes core–hole effects, dash-dot line does not include core–hole effects.

good agreement with experiment can be achieved for these covalent compounds if the core–hole effects are taking into account. These calculations reproduce all details present in the fine structure in terms of number of peaks, peak intensity and peak position. When the core–hole effects are not considered in the calculation the fine structure spreads over a broader energy range with different peak intensity and position as it is expected.

Clear differences between both materials can be observed in all these edges. In fact, the spectra show important differences in the fine structure present in the first 10 eV and also at higher energies in both the experimental and calculated spectra.

For the S-K edge the fine structure in both materials consists of an intense peak about 5 eV wide. In MgS an additional peak is present at about 6 eV above the first maximum. The first peak is composed of a three-peak structure, with a different relative intensity in both compounds that is responsible for the different shape of this peak in MgS and $MgYb_2S_4$. For the Mg-K edge the fine structure observed within the first 8 eV above threshold consist of a 3 peaks structure with similar relative intensities but different peak energy (peak position). Other differences appear at higher energies in both edges in the form of different number of peaks and in their

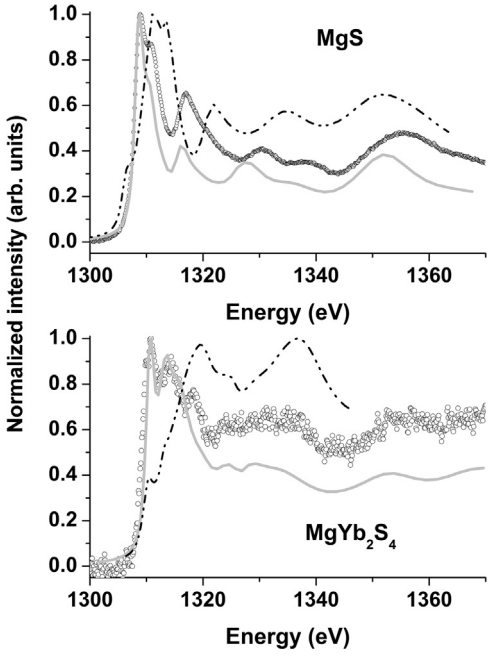

Fig. 4. Mg K-edge in MgS and $MgYb_2S_4$. Experimental: open circles. Calculated: solid gray line includes core–hole effects, dash-dot line does not include core–hole effects.

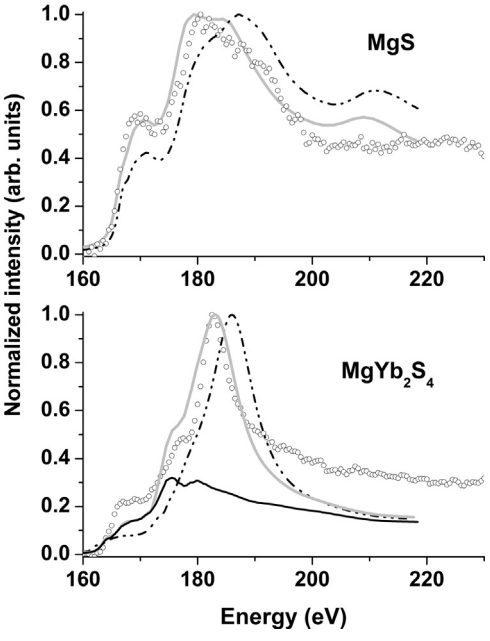

Fig. 6. S $L_{2,3}$-edges in MgS and S $L_{2,3}$- and Yb N_5-edges in $MgYb_2S_4$. Experimental: open circles. Calculated: solid gray line includes core–hole effects, dash-dot line does not include core–hole effects.

energy position. Such differences are more clear in the S-K edge. Since these features seem to be multiple scattering resonances, which should go as 1/(bond length)^2 we attribute these differences to the different crystal structures, with distinct S-Mg nearest neighbor distances: 0.26 and 0.236 for MgS and $MgYb_2S_4$ respectively, and 0.2725 for S-Yb.

These clear differences in the near-edge structure (ELNES) reflect the different structural environments in MgS and $MgYb_2S_4$ and the different electronic structure of $MgYb_2S_4$ as discussed above. The electronic states that contribute to each peak can be deduced from the previous discussion of the DOS. Note that the core–hole effects in Mg K-edge is more significant than in S K-edge, in agreement with Gao et al. (2008). The observed features should allow us to identify and distinguish between these phases.

In Figs. 5 and 6 other delayed edges like the $L_{2,3}$ edges of Mg and S and Yb N_5 edge are shown. Important differences are clear between the two compounds in both figures.

In Fig. 5 we can see that these two Mg $L_{2,3}$-spectra are dissimilar because in MgS a strong peak at threshold is observed whilst this peak is not observed in $MgYb_2S_4$. In the spinel these edges have a delayed shape. Although the calculation including core–hole effects gives a better average agreement with the experiment, it predicts a higher intensity at threshold, at about 48–50 eV, than the observed. The comparison of experiment and calculation at this energy range is related to the detection of the very weak features at threshold which in delayed edges is usually very sensitive to background subtraction. Background estimation is more difficult in very shallow edges like the current one because of the presence of intense tails from low loss features. Our energy resolution also introduces an added difficulty to detection of weak features at threshold. Thus, we think the discrepancy between experiment and calculation can be attributed to these factors. The intense and narrow peak at threshold in MgS is similar to those reported for MgO and $MgAl_2O_4$ which was identified as a core exciton in these wide band gap materials (O'Brien et al., 1991, 1993). The reduced band gap of $MgYb_2S_4$ could explain the absence of this peak. The peak intensity in the vicinity of the edge threshold is underestimated in the calculated spectrum. A proper calculation of the excitonic effect should involve two-particle calculations (Mizoguchi et al., 2010).

In Fig. 6 are shown the S $L_{2,3}$-edges. For the spinel the Yb N_5-edge is overlapping with those of sulfur. These edges can also be used to distinguish between both compounds, as those of previous figures. However there is not much fine structure information in the sulfur edges. For $MgYb_2S_4$ the Yb contribution dominates the whole spectrum. The sulfur edges are plotted in order to distinguish the Yb contribution which consists of just one intense peak.

In consequence these spectra confirm they can be used as end members for an empirical fingerprinting of composition changes in the solid solution. The K-edges are the sensitive ones to the local coordination. The good agreement found between experiment and calculations demonstrate the suitability of FEFF for the study of these sulfides.

5. Conclusions

We have measured by EELS the S K-, S $L_{2,3}$-, Mg K-, Mg $L_{2,3}$- and Yb N_5-edges present in MgS and $MgYb_2S_4$ compounds and used FEFF9.6 program for the theoretical analysis of these EEL spectra. It was found a very good agreement between experimental and calculated spectra for both edges when the core–hole effects are included in the calculation. The fine structure observed can be used to fingerprint each material. Our calculations indicate that the valence band of MgS is dominated by S states, the 2p states contributing to the top of the band and the S 2s states to the bottom of the band. The conduction band is equally contributed by Mg and S states. For $MgYb_2S_4$ contributions by Mg and S have a similar distribution, the main difference being the Yb states, which dominate the top of the valence band and are the more important contributor up to 10 eV above Fermi level. A narrower band gap (compared to MgS) is predicted for this material.

Acknowledgements

M.S.M. thanks the partial financial support of CONICET, Argentina. LCOD and EUG thank the financial support from the project MAT-2013-44964-R-SPAIN.

References

Ankudinov, A.L., Ravel, B., Rehr, J.J., Conradson, S.D., 1998. Real-space multiple-scattering calculation and interpretation of x-ray-absorption near-edge structure. Phys. Rev. B 58, 7565–7576.
Barrett, E., Fern, G.R., Ray, B., Withnall, R., Silver, J., 2005. UV photoluminescence from small particles of calcium cadmium sulfide solid solutions. J. Opt. A: Pure Appl. Opt. 7, S265–S269.
Cai, K., Song, M.-K., Cairns, E.J., Zhang, Y., 2012. Nanostructured Li_2S–C composites as cathode material for high-energy lithium/sulfur batteries. Nano Lett. 12, 6474–6479.
Chen, Z.J., Zu, X.T., Wang, Y.X., Xue, S.W., 2009. Electronic and optical properties of pure and Ce^{3+}-doped MgS single crystals: a first-principles prediction. J. Appl. Phys. 105 (art. no 063532).
Drief, F., Tadjer, A., Mesri, D., Aourag, H., 2004. First principles study of structural, electronic, elastic and optical properties of MgS, MgSe and MgTe. Catal. Today 89, 343–355.
Egerton, R.F., 2011. Electron Energy-Loss Spectroscopy in the Electron Microscope. Springer, New York.
Flahaut, J., 1979. Sulfides, selenides and tellurides. In: Gschneider, K.L., Eyring, L. (Eds.), Handbook on the Physics and Chemistry of Rare Earths, 4. North-Holland, Amsterdam, pp. 1–88.
Fleet, M.E., 2005. Xanes spectroscopy of sulfur in earth materials. Can. Mineralogist 43, 1811–1838.
Gao, M.-R., Xu Jiang, J., Yu, S.-H., 2013. Nanostructured metal chalcogenides: synthesis, modification, and applications in energy conversion and storage devices. Chem. Soc. Rev. 42, 2986–3017.
Gao, S.-P., Pickard, C.J., Payne, M.C., Zhu, J., Yuan, J., 2008. Theory of core–hole effects in 1*s* core-level spectroscopy of the first-row elements. Phys. Rev. B 77 (art. no. 115122).
Jorissen, K., Rehr, J.J., 2010. Calculations of electron energy loss and x-ray absorption spectra in periodic systems without a supercell. Phys. Rev. B 81 (art. no. 245124).
Johari, P., Shenoy, V.B., 2012. Tuning the electronic properties of semiconducting transition metal dichalcogenides by applying mechanical strains. ACS Nano 6, 5449–5456.
Kalpana, G., Palanivel, B., Thomas, R.M., Rajagopalan, M., 1996. Electronic and structural properties of MgS and MgSe. Phys. B 222, 223–228.
Khan, I., Afaq, A., Aliabad, H.A.R., Ahmad, I., 2012. Transition from optically inactive to active Mg-chalcogenides: a first principle study. Comput. Mater. Sci. 61, 278–282.
Kravtsova, A.N., Stekhin, I.E., Soldatov, A.V., Liu, X., Fleet, M.E., 2004. Electronic structure of MS (M = Ca,Mg,Fe. Mn): X-ray absorption analysis. Phys. Rev. B 69 (art. no.134109).
Lavrentyev, A.A., et al., 2011. Electronic structure of $ZrTiO_4$ and $HfTiO_4$: self-consistent cluster calculations and X-ray spectroscopy studies. J. Phys. Chem. Solids 72, 83–89.
Mizoguchi, T., Olovsson, W., Ikeno, H., Tanaka, I., 2010. Theoretical ELNES using one-particle and multi-particle calculations. Micron 41, 695–709.
Moreno, M.S., Jorissen, K., Rehr, J.J., 2007. Practical aspects of electron energy-loss spectroscopy (EELS) calculations using FEFF8. Micron 38, 1–11.
O'Brien, W.L., Jia, J., Dong, Q.-Y., Callcott, T.A., Mueller, D.R., Ederer, D.L., Kao, C.-C., 1993. Soft-X-ray investigation of Mg and Al oxides: evidence for atomic and bandlike features. Phys. Rev. B 47, 15482–15486.
O'Brien, W.L., Jia, J., Dong, Q.-Y., Callcott, T.A., Rubensson, J-E., Mueller, D.R., Ederer, D.L., 1991. Intermediate coupling in L2–L3 core excitons of MgO, $A1_2O_3$, and SiO_2. Phys. Rev. B 44, 1013–1018.
Poole, I.B., Ng, T.L.T.L., Maung, N., Williams, N., Wright, J.O.A.C., 1997. MOVPE growth of magnesium cadmium sulphide rocksalt or sphalerite? J. Cryst. Growth 170, 528–532.
Rehr, J.J., Kas, J.J., Vila, F.D., Prange, M.P., Jorissen, K., 2010. Parameter-free calculations of X-ray spectra with FEFF9. Phys. Chem. Chem. Phys. 12, 5503–5513.
Smet, P.F., Moreels, I., Hens, Z., Poelman, D., 2010. Luminescence in sulfides: a rich history and a bright future. Materials 3, 2834–2883.
Stepanyuk, V.S., et al., 1992. Electronic structure and optical properties of MgS. Phys. Stat. Sol. (b) 174, 289–294.

Su, Y.-S., Manthiram, A., 2012. Lithium–sulphur batteries with a microporous carbon paper as a bifunctional interlayer. Nat. Commun. 3, 1166.

Urones-Garrote, E., Gómez-Herrero, A., Landa-Cánovas, A.R., Fernández-Martinez, F., Otero-Díaz, L.C., 2004. Synthesis and characterization of possible pigments in the Mg–Yb–S system. J. Alloys Compd. 374, 197–201.

Urones-Garrote, E., Gómez-Herrero, A., Landa-Cánovas, A.R., Withers, R.L., Otero-Díaz, L.C., 2005. Order and disorder in rocksalt and spinel structures in the MgS–Yb_2S_3 system. Chem. Mater. 17, 3524–3531.

Withers, R.L., Urones-Garrote, E., Otero-Díaz, L.C., 2007. Structured diffuse scattering, local crystal chemistry and metal ion ordering in the $(1-x)$MgS·x/3Yb2S3, $0 \leq x \leq \sim 0.45$, 'defect' NaCl system. Phil. Mag. 87, 2807–2813.